THE JOURNAL OF PHYSICAL CHEMISTRY C

Article

pubs.acs.org/JPCC

Catalytic Dehydration of 2-Propanol by Size-Selected $(WO_3)_n$ and $(MoO_3)_n$ Metal Oxide Clusters

Xin Tang,[†] Dennis Bumueller,[‡] Alane Lim,[†] John Schneider,[‡] Ulrich Heiz,[§] Gerd Ganteför,[‡] D. Howard Fairbrother,*[,†] and Kit H. Bowen*[,†]

[†]Department of Chemistry, Johns Hopkins University, Baltimore, Maryland 21218, United States

[‡]Department of Physics, University of Konstanz, 78457 Konstanz, Germany

[§]Department of Chemistry − Catalysis Research Center, Technische Universität München, 85748 Garching, Germany

Supporting Information

ABSTRACT: Here, we report the catalytic dehydration of 2-propanol by metal oxide clusters, $(WO_3)_n$ and $(MoO_3)_n$ (n = 1, 2, 3, 5, 30), prepared by mass selecting and soft-landing metal oxide cluster anions created in the gas phase. Temperature-programmed reaction (TPR) was used to characterize the catalytic activity of the deposited clusters by measuring the production of propene from 2-propanol. The nature of the support, thermal history, size of the cluster, and cluster composition were all found to play important roles in influencing catalytic activity. $(WO_3)_3$ clusters deposited on HOPG (highly ordered pyrolytic graphite) and oxide supports exhibited catalytic activity, although $(WO_3)_1$ monomers deposited on HOPG did not catalyze 2-propanol dehydration effectively, an effect ascribed to their coalescence into large aggregates on HOPG. For tungsten oxide clusters deposited on annealed oxide films, catalytic activity was observed for all cluster sizes and was linearly correlated with the size of the deposited clusters. Two different mechanisms, linear-scaling of active sites and cluster ripening, could account for this linear dependence. However, even on oxide supports, deposited tungsten oxide clusters lost catalytic activity after annealing to 400 °C. The effect is consistent with the loss of dioxo groups rather than any cluster aggregation. Compared to tungsten oxide clusters, molybdenum oxide clusters exhibited little or no catalytic activity toward the dehydration of 2-propanol, rationalized by the decrease in Lewis acidity of molybdenum−oxygen bonds.

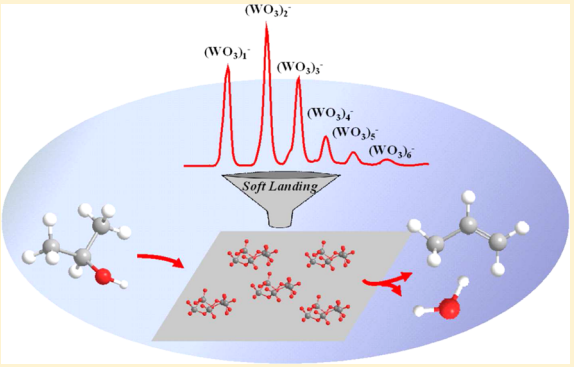

I. INTRODUCTION

Clusters are assemblies of atoms and molecules with sizes ranging from subnanometer to a few nanometers. Because the size of clusters falls into the nonscalable region, many of their properties, that is, electron structures, geometric structures, magnetic properties, and so on, are strongly dependent on their size.[1,2] As catalysts, clusters also exhibit size dependent catalytic properties. For example, Au_n clusters deposited on magnesia thin films were found to induce CO oxidation starting at n = 8.[3,4] Likewise, studies of Pd_n clusters deposited on $TiO_2(110)$ were found to show strong size effects during CO oxidation.[5] The correlation between the cluster size and catalytic activity suggests a novel way for tuning catalytic activities, that is, by selecting specific cluster sizes.

To generate size-selected cluster catalysts, mass spectrometric methods such as quadruple mass spectrometry,[5−8] time-of-flight (TOF),[9,10] and magnetic sector mass spectrometry[11,12] have been used to mass-select cluster ions, followed by soft-landing them onto supports. For heterogeneous catalysis studies, these mass-selected clusters have several advantages over those synthesized by other methods. Compared to nanoclusters synthesized by solution[13] or sol−gel methods,[14] soft-landed, mass-selected clusters are free of stabilizers, such as ligands and surfactants that could complicate or even block catalytic active sites. Compared to methods such as physical vapor deposition (PVD)[15,16] or chemical vapor deposition (CVD),[17] mass-selected cluster deposition allows for "atom by atom" control of cluster size and composition, critical to the ability to tune the catalytic activity of many cluster catalysts. Additionally, when the number of atoms in mass-selected clusters is relatively small, high-level quantum calculations can be applied to elucidate their structure in the presence or absence of underlying supports.[4,18] Consequently, the examination of catalytically active sites, for example, steps, and their corresponding electronic properties, may also be computationally tractable.

Special Issue: John C. Hemminger Festschrift

Received: June 2, 2014
Revised: July 17, 2014
Published: July 21, 2014

dx.doi.org/10.1021/jp505440g | J. Phys. Chem. C 2014, 118, 29278−29286

In contrast to studies on size-selected metal cluster catalysts, there is a relative paucity of information on the properties of metal oxide clusters. Examples include studies of the structures of vanadium oxide clusters on rutile $TiO_2(110)$ surfaces[19] and investigations on the stabilities of cobalt oxide clusters on diamond and alumina supports.[20] In addition, our group has studied the structure of molybdenum oxide,[12,21] tungsten oxide,[21] and titanium oxide clusters[22] formed from size-selected clusters deposited on HOPG (highly ordered pyrolytic graphite) surfaces. Other researchers have used PVD to deposit small tungsten oxide and molybdenum oxide clusters (predominantly trimers) onto $TiO_2(110)$ and other supports and studied their catalytic dehydration, dehydrogenation, and condensation properties.[23−27] Systematic, size-dependent cluster catalyst studies, however, are not possible with thermal methods of evaporation. In related gas phase studies, the reaction products formed by collisions between small, mass-selected molybdenum suboxide cluster anions and water molecules were shown to be dependent on the number of molybdenum atoms in the cluster.[28] Gas-phase, metal oxide cluster anions have also been studied via anion photoelectron spectroscopy, and several of these have been investigated theoretically.[29−32] Together, anion photoelectron spectroscopy and theory can uncover both the electronic and the geometric structure of clusters as a function of their size and composition. This is important because both reactivity and catalytic activity depend strongly on electronic and geometrical structure.[33,34] Moreover, previous studies have shown that the ultimate structure of deposited clusters, including the propensity for cluster aggregation and site-specific nucleation are regulated by cluster size, composition, deposition rate, and the nature of the support.[11,12,22,35,36] All of these variables will play a role in determining both the electronic and geometrical structure of the deposited clusters with likely impacts on the reactivity and catalytic activity of the clusters. The present study explores the catalytic dehydration of 2-propanol using mass-selected $(MoO_3)_n$ and $(WO_3)_n$ clusters deposited on two different substrates, HOPG and an annealed metal oxide. This catalytic activity was studied using temperature-programmed reaction (TPR) to probe the formation of propene from 2-propanol.

II. EXPERIMENTAL METHODS

In this work, metal oxide clusters were produced as anions by a magnetron source. After mass selection and deceleration, they were then deposited (soft-landed) onto a substrate in an ultra-high vacuum (UHV) environment (1×10^{-9} Torr). In the magnetron source, a metal target was placed in a magnetic field and biased to −500 V, where a mixture of argon, helium and oxygen gases was also present. The argon gas was ionized to create argon cations, which in turn sputtered the metal target to produce metal atoms and electrons. Upon reaction with oxygen to form oxides, these metal oxides aggregated, attached electrons, and formed metal oxide cluster anions. The added helium served to cool and transport the cluster anions downstream, where they were accelerated before entering a magnetic sector mass spectrometer (25° sector magnet with resolution of $m/\Delta m = 20$). By tuning the magnetic field strength, $(WO_3)_n^-$ (n = 1, 2, 3, 5, 30) and $(MoO_3)_n^-$ (n = 1, 2, 3, 5, 30) cluster anions were mass-selected and focused by ion optics before entering the deposition chamber, where they were soft-landed (kinetic energy < 0.1 eV/atom) onto a freshly peeled HOPG surface. The sample was cooled to approximately −160 °C by liquid nitrogen (LN_2) during cluster deposition and could be heated by passing current through a tantalum plate mounted behind and attached to the sample (i.e., resistive heating). The temperature of the sample was monitored by a K-type thermocouple attached to the back of the sample holder. Upon deposition, clusters are presumed to lose their excess charge to the conductive surface and to become neutral clusters. The number of clusters deposited on surface is calculated by integrating the cluster current over the deposition time. By assuming a cluster sticking coefficient of unity, a monolayer of WO_3 will require 2.6×10^{14} clusters for the case of $(WO_3)_1$ monomer. Details of the source and deposition chamber can be found in refs 12 and 21, and a schematic is provided as Figure S1 in the Supporting Information.

Once clusters had been deposited onto the HOPG substrate, a TPR setup, using a Hiden HAL/3F PIC quadruple mass spectrometer (QMS), was used to characterize their catalytic activity. After cluster deposition, the sample temperature was increased to 25 °C, at which point 2-propanol was adsorbed. This allowed for the chemisorption of 2-propanol onto oxides instead of the formation of physisorbed 2-propanol at low temperatures.[24] The 2-propanol was purified by several freeze−pump−thaw cycles before being background dosed through a UHV compatible leak valve. Unless noted, 0.2 L propanol was dosed (2×10^{-9} Torr for 100 s). Once the 2-propanol had been adsorbed, the sample was cooled to −50 °C and then heated to 400 °C, with a temperature ramping rate of 2 °C/s. The sample was cooled after 2-propanol adsorption to ensure a flat baseline by starting the temperature ramp well below the 2-propanol desorption temperature. The reaction products desorbed from the surface during the temperature ramp were detected and identified by the QMS, which was positioned normal to the plane of the substrate and at a distance of 5 mm. To minimize the contribution from background gases and maximize the sensitivity toward species desorbing directly from the substrate, the QMS ionizer was surrounded by a custom built glass shroud. Thus, in a typical experimental run, both 2-propanol and the mass-selected metal oxide cluster anions were codeposited onto a substrate in a sequential fashion, which was then subsequently heated. Samples could also be transferred to an adjacent UHV chamber, where they were characterized by X-ray photoelectron spectroscopy (in situ XPS) with non-monochromatic Mg Kα rays (1253.6 eV) and analyzed with a high energy electron analyzer. The structures of the deposited clusters were also characterized ex situ by atomic force microscopy (AFM). AFM images were acquired using a PicoSPM LE AFM (Agilent Technologies) operated in magnetic tapping mode using Co−Cr tips obtained from MikroMasch (NSC18). In principle, AFM tips could pick up and move loosely bound clusters adsorbed onto a surface. This potential issue was addressed by verifying that the AFM images remained unchanged after the same region was repeatedly imaged.

III. RESULTS

Mass Spectra and XPS Characterization of Metal Oxide Clusters. Figure 1 shows the mass spectra of both the tungsten oxide (a) and molybdenum oxide (b) cluster anions used in this work. Both mass spectra show individually well-resolved peaks for the smaller ($n \leq 10$) metal oxide cluster sizes. Therefore, by appropriately tuning the mass filter we can size-select different clusters for deposition. Once deposited, the chemical composition of these clusters was characterized by in

dx.doi.org/10.1021/jp505440g | J. Phys. Chem. C 2014, 118, 29278−29286

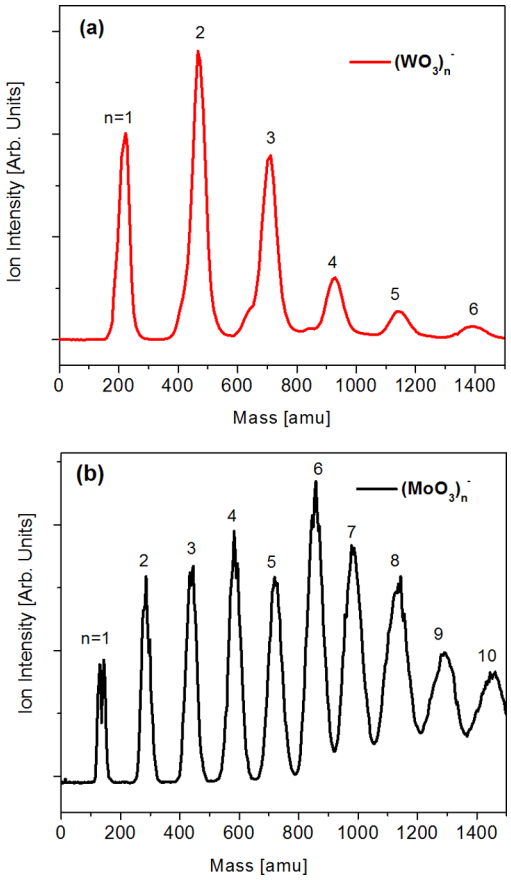

Figure 1. Mass spectra of (a) $(WO_3)_n$ and (b) $(MoO_3)_n$ cluster anions.

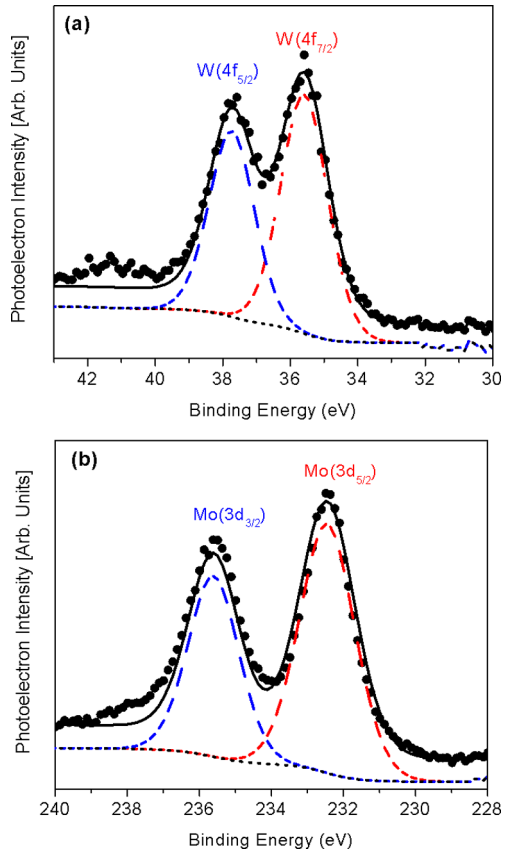

Figure 2. In situ XPS envelopes of (a) W(4f) region for $(WO_3)_n$ clusters and (b) Mo(3d) region for $(MoO_3)_n$ clusters deposited on HOPG.

situ XPS, as shown in Figure 2. For the tungsten oxide clusters shown in Figure 2a, the XP spectral envelope in the W (4f) region shows two peaks, that is, W $4f_{5/2}$ and W $4f_{7/2}$, with their peak positions centered at 37.7 and 35.6 eV, respectively. The binding energy of W $4f_{7/2}$ indicates that W is in its highest oxidation state, that is, VI.[21,37] Meanwhile, the XP spectral envelope in the Mo (3d) region in Figure 2b also shows a doublet, that is, Mo $3d_{3/2}$ and Mo $3d_{5/2}$, with peak positions centered at 235.6 and 232.5 eV, respectively. The binding energy of the Mo $3d_{5/2}$ peak confirms that molybdenum atoms are also in their highest (VI) oxidation state.[21,38]

TPR of 2-Propanol on $(WO_3)_n$ Clusters. Figure 3a,b show the TPR traces of 0.2 L of 2-propanol adsorbed on HOPG both without and with deposited $(WO_3)_3$ clusters, respectively. In the absence of $(WO_3)_3$ clusters, Figure 3a shows that the main desorption products detected by the QMS were 2-propanol's fragmentation products at m/z = 45, 41, and 43 amu, consistent with measurements of gas-phase 2-propanol. Since all three species originate from desorbed 2-propanol, they exhibit coincident desorption profiles. However, when $(WO_3)_3$ clusters were deposited onto the HOPG surface, Figure 3b reveals that a new, higher temperature, peak appears at m/z = 41 amu in the absence of any corresponding peaks at m/z = 45 amu and m/z = 43 amu. Since the peak at m/z = 41 amu is the major fragmentation peak for propene, we assign this peak to the production of propene as a result of reactions between 2-propanol and the deposited $(WO_3)_3$ clusters (Other major propene fragmentation products at m/z = 39, 42, 27, 40 amu were also observed, verifying this assignment). Once the contribution to the m/z = 41 amu trace from 2-propanol desorption at lower temperatures was subtracted, a symmetric propene desorption profile is observed (see Figure 3d). Examples of this deconvolution procedure are shown in the Supporting Information (Figure S2). The desorption temperature of propene is about 190 °C, higher than the propene desorption temperature (127 °C) observed in previous studies when 2-propanol reacts with $(WO_3)_3$ clusters deposited on $TiO_2(110)$.[23] Since a different temperature ramp rate (1.8 °C/s) was used in the two studies, a Redhead analysis[39] was necessary to compare the desorption energy of propene. Assuming a frequency factor $\nu_1 = 10^{13}$ s^{-1}, the calculated desorption energies of propene from $(WO_3)_3$ clusters adsorbed on HOPG and $TiO_2(110)$ are 29.2 and 25.2 kcal/mol, respectively, close to the predicted value (26−28 kcal/mol) for propene formation from 2-propanol on $(WO_3)_3$ clusters.[23]

Figure 4 displays TPR traces for propene production as a function of the total number of $(WO_3)_3$ clusters deposited on HOPG, each sample having been dosed with 0.2 L of 2-propanol. As the number of clusters increased, the propene desorption temperature remained almost constant at around 190 (±5) °C although the propene peak area increased. Moreover, analysis of the propene peak area plotted as a function of the number of $(WO_3)_3$ clusters deposited reveals a linear correlation between the total number of clusters deposited and the propene yield (see inserted figure in Figure 4).

Figure 5a,b shows TPR traces of propene production for $(WO_3)_3$ clusters adsorbed on HOPG before and after annealing to 400 °C, respectively. Before annealing, $(WO_3)_3$ clusters were

dx.doi.org/10.1021/jp505440g | J. Phys. Chem. C 2014, 118, 29278−29286

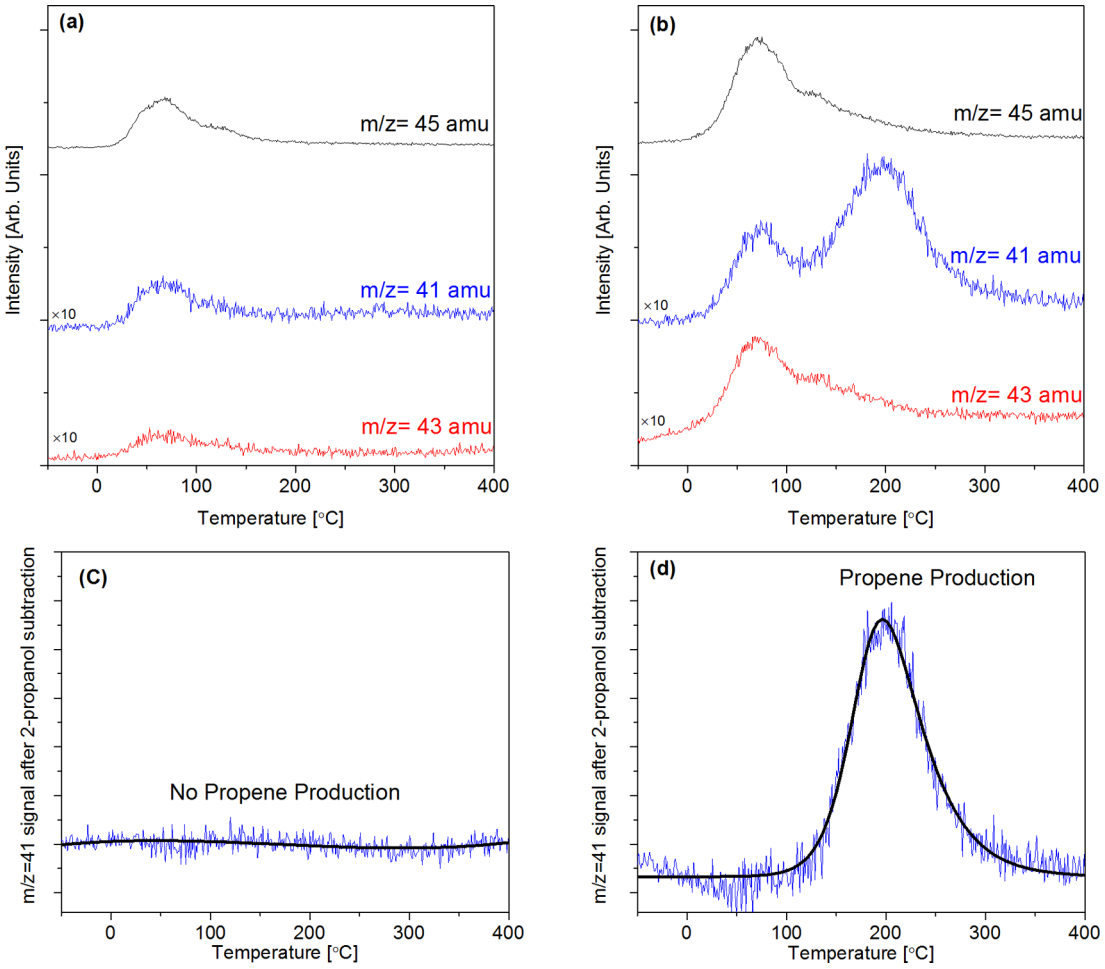

Figure 3. TPR traces of 2-propanol on HOPG (a) without deposited $(WO_3)_3$ clusters and (b) with deposited $(WO_3)_3$ clusters. m/z = 41 amu signal after subtraction of the 2-propanol contribution for HOPG (c) without deposited $(WO_3)_3$ clusters and (d) with deposited $(WO_3)_3$ clusters.

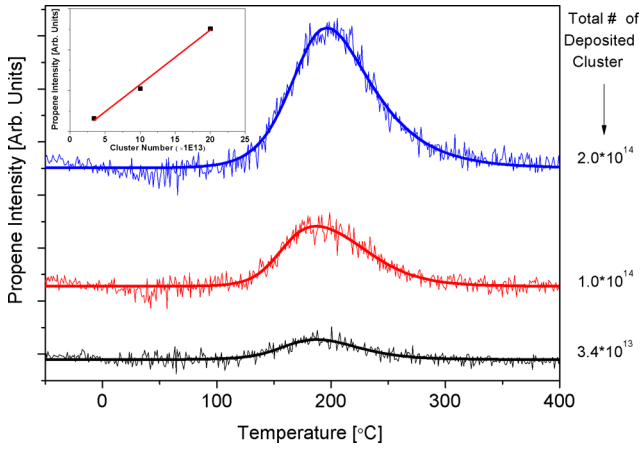

Figure 4. TPR traces of propene production vs the number of $(WO_3)_3$ clusters deposited on HOPG. Inset shows a linear fitting between the propene yield vs the number of $(WO_3)_3$ clusters deposited on HOPG.

active for propene production. However, after annealing, the same clusters were no longer active toward propene production (92% loss of the catalytic activity). AFM was used to determine the structures of the as-deposited clusters as well as the effect of annealing, shown in Figure 5c and d, respectively. For the as-deposited $(WO_3)_3$ clusters, Figure 5c showed some degree of aggregation indicating the mobility of $(WO_3)_3$ clusters on HOPG surface, as expected for small sized clusters on HOPG.[21] The cluster aggregates are about 0.5−0.6 nm in height and their sizes are as large as several tens of nanometers revealed from the line scan shown in Figure 5e. Therefore, the $(WO_3)_3$ clusters deposited on HOPG aggregated into mostly two-dimensional structures. However, no strong step-edge preference for cluster nucleation on the HOPG surface was observed, suggesting that clusters become immobilized once they have aggregated. Most importantly, in the context of the present investigation, the surface structure did not change visibly after annealing to 400 °C.

To investigate the support effect on the cluster activity, $(WO_3)_1$ was deposited onto two different supports, i.e., HOPG and annealed tungsten oxide films, and their catalytic activity was compared. Figure 6a(I) shows $(WO_3)_1$ monomers deposited on HOPG, while Figure 6a(II) shows $(WO_3)_1$ monomers deposited on annealed WO_3 films. As can be seen in Figure 6a(I), $(WO_3)_1$ monomers deposited on HOPG are relatively inactive. However, on annealed WO_3 films, deposited $(WO_3)_1$ monomers became active, as seen in Figure 6a(II) (the propene peak area is at least five times larger for $(WO_3)_1$ monomers deposited on HOPG[40]). Thus, annealed oxide films are a significantly better support for promoting catalytically active tungsten oxide clusters.

Figure 6a(II−VI) presents TPR traces of propene production as a function of cluster size for $(WO_3)_n$ (n = 1, 2, 3, 5, 30)

dx.doi.org/10.1021/jp505440g | J. Phys. Chem. C 2014, 118, 29278−29286

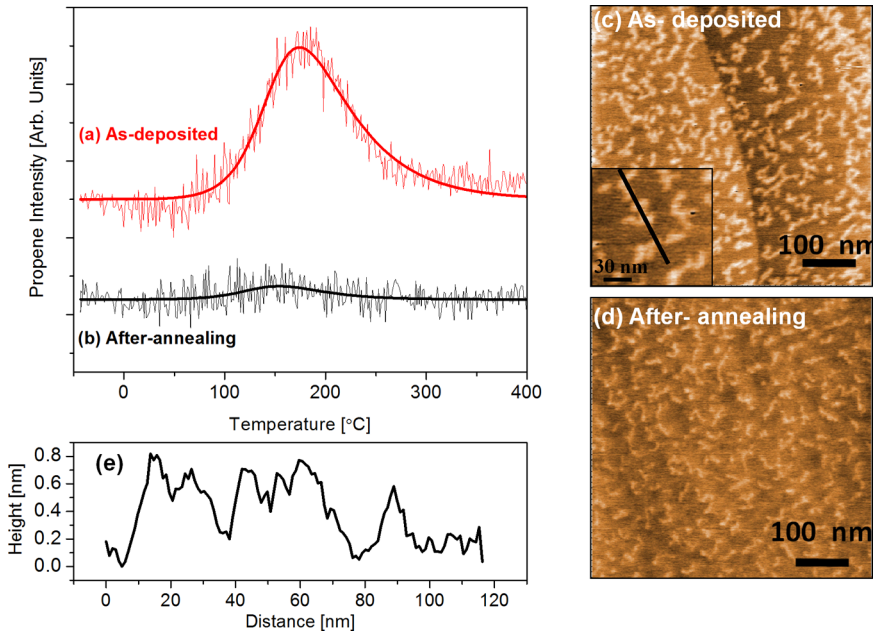

Figure 5. TPR traces of propene production of $(WO_3)_3$ clusters deposited on HOPG (a) as-deposited and (b) after annealing to 400 °C; corresponding AFM images of the (c) as-deposited (inset shows a magnified image of the cluster aggregates) and (d) after annealing $(WO_3)_3$ clusters deposited on HOPG; (e) A line scan of cluster aggregates along the black solid line shown in (c).

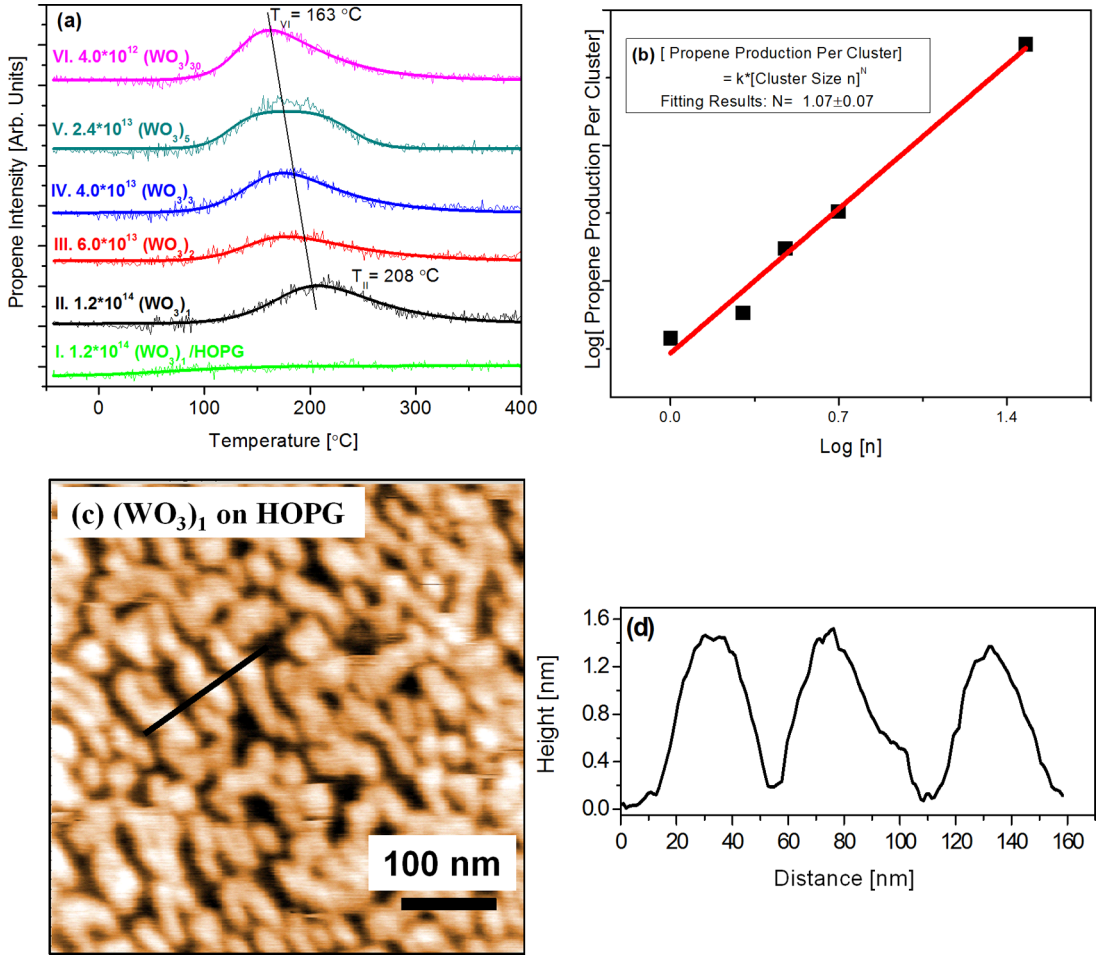

Figure 6. (a) TPR traces of propene production for (I) $(WO_3)_1$ clusters deposited on HOPG and (II–VI) $(WO_3)_n$ clusters deposited on annealed WO_3 films (n = 1, 2, 3, 5, 30) after dosing 0.2 L propanol; (b) Plot of Log[propene production per $(WO_3)_n$ cluster] vs Log [cluster size n]; (c) AFM image of $(WO_3)_1$ monomers deposited on HOPG; (d) A line scan of cluster aggregates along the black solid line shown in (c).

dx.doi.org/10.1021/jp505440g | J. Phys. Chem. C 2014, 118, 29278–29286

clusters deposited on annealed tungsten oxide films. All of these cluster sizes are active toward propene production. For each trace, the total number of W atoms deposited is the same. This was accomplished by ensuring that the total number of deposited clusters times that cluster's size (n number) was kept constant between different experiments. The propene desorption peak area for all the different sizes of clusters on the annealed oxide films displayed a similar value irrespective of the cluster size. This implies a correlation between the propene yield and the number of tungsten atoms involved in catalysis. Thus, a log−log fitting was applied to extrapolate the order of dependence. Indeed, by plotting Log[propene production per cluster] versus Log[cluster size n], as shown in Figure 6b, the gradient (N) is very close to 1 ($N = 1.07 \pm 0.07$), indicating a linear correlation exists.

Figure 7 displays the TPR traces for propene production for $(MoO_3)_3$ clusters and $(MoO_3)_1$ monomers deposited on

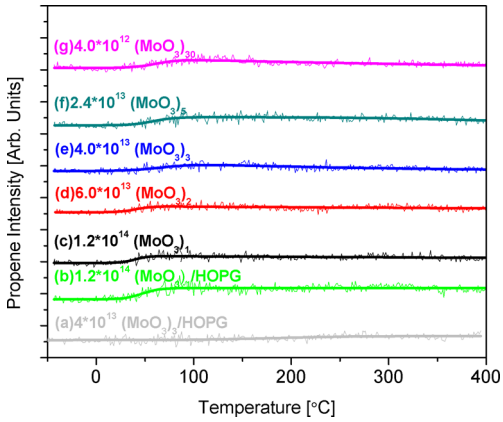

Figure 7. TPR traces of propene production for (a) $(MoO_3)_3$ and (b) $(MoO_3)_1$ clusters deposited on HOPG and (c−g) $(MoO_3)_n$ clusters deposited on annealed MoO_3 films (n = 1, 2, 3, 5, 30) (Note the y-axis scale is the same as the one in Figure 6a).

HOPG (Figure 7a,b) and $(MoO_3)_n$ clusters deposited on annealed MoO_3 films (Figure 7c−g). In contrast to the behavior of $(WO_3)_n$ clusters, these TPR traces show that none of the $(MoO_3)_n$ clusters are catalytically active for 2-propanol dehydration to form propene, regardless of their size or the nature of the support.

IV. DISCUSSION

Dehydration of 2-Propanol on $(WO_3)_3$ Clusters. In previous studies, Dohnálek et al. studied the catalytic dehydration of 2-propanol due to $(WO_3)_3$ trimers adsorbed on $TiO_2(110)$.[23] Through the use of IR spectroscopy and desorption measurements, the catalytic activity of these clusters was proposed to be a consequence of the presence of the O═W═O dioxo group within the cluster.[26] Computational results also suggested that the dioxo groups were the favored sites for alcohol dehydration because of the greater Lewis acidity of these groups as compared to the monooxo groups, which translated into a lower activation energy barrier for alcohol dehydration via C−H and C−O bond cleavage.[26]

Results from the present investigation (Figure 3b) show that, as-deposited, mass-selected $(WO_3)_3$ clusters on HOPG are similarly catalytically active toward 2-propanol dehydration although they aggregate into cluster-island structures, as shown in Figure 5c. As seen in Figure 4, increasing the number of $(WO_3)_3$ clusters on the surface linearly increases propene production without changing the peak position indicating a linear increase of the accessible active sites in the cluster-island aggregates. These observations are qualitatively consistent with those of Dohnálek et al.[23] Annealing of the as-deposited clusters, however, leads to the 92% loss of catalytic activity as shown in Figure 5b. In principle, this loss of activity might be a result of $(WO_3)_3$ clusters sintering on the HOPG surface during TPR heating, a phenomenon commonly observed for small clusters on HOPG surfaces.[41] However, as shown in Figure 5c,d, the AFM images acquired both before and after annealing did not exhibit dramatic changes in the surface morphology of the deposited clusters. Thus, aggregation effects do not appear to be responsible for the loss of activity. The likely interpretation, suggested by Dohnálek et al.[26] on the basis of IR data and desorption measurements is that annealing tungsten oxide results in the conversion of O═W═O dioxo groups into catalytically inactive W═O monooxo groups leading to a loss of catalytic activity. In this respect, a dioxo to monooxo bonding transformation would not necessarily change the surface morphology, but would diminish the catalytic activity of the clusters.

Influence of the Substrate. To probe the influence of the substrate, the activity of the $(WO_3)_1$ monomer was studied on two different substrates, that is, on HOPG and on annealed WO_3 oxide films. Since annealed WO_3 oxide films themselves were shown to be catalytically inactive for 2-propanol dehydration (see Figure 5b), they were chosen as a point of comparison with HOPG substrates, which are also inactive toward 2-propanol dehydration in the absence of adsorbed clusters (see Figure 3a). Our results showed that $(WO_3)_1$ deposited on HOPG did not catalyze the dehydration reaction effectively, while the same quantity of $(WO_3)_1$ clusters deposited on annealed oxide films were catalytically active. [See (I) and (II) in Figure 6a.] Generally, small clusters are extremely mobile on HOPG surfaces, and due to a combination of their mobility and high surface energy, they coalesce into larger aggregates with a reduced surface area[42] and a commensurate loss of catalytically active sites. Indeed, significant cluster aggregation is observed on HOPG in the case of deposited $(WO_3)_1$ monomers (see Figure 6c). As shown in Figure 6d, $(WO_3)_1$ monomers aggregated three dimensionally on HOPG surface and coalesced into nanoparticles of about 1.5 nm in height. In contrast, much less cluster coalescence is observed for $(WO_3)_3$ clusters deposited on HOPG (compare Figure 5c and 6c; Figure 5e and Figure 6d). This difference in aggregation behavior as a function of cluster size would explain the difference in reactivity between $(WO_3)_1$ and $(WO_3)_3$ deposited on HOPG. On the annealed WO_3 surface, we speculate that $(WO_3)_1$ becomes physically trapped or otherwise anchored, perhaps due to surface defects, preventing agglomeration. This is consistent with STM data from Dohnálek et al.[43] showing that $(WO_3)_3$ clusters deposited by PVD are immobilized on $TiO_2(110)$ surfaces, suggesting that the strength of interaction between tungsten oxide clusters and an underlying oxide surface will also be sufficiently large in magnitude to immobilize the clusters in the absence of significant aggregation and agglomeration. Unfortunately, direct imaging of the deposited clusters on annealed tungsten oxide surfaces by AFM is complicated by the roughness of the oxide support (see Figure S3).

Analogous to the comparative study of $(WO_3)_1$, we compared 2-propanol dehydration reactions for $(WO_3)_3$

dx.doi.org/10.1021/jp505440g | J. Phys. Chem. C 2014, 118, 29278−29286

deposited on HOPG and annealed oxide films, shown in Figures 4 and Figure 6a(IV), respectively. For the same quantity of deposited $(WO_3)_3$ clusters, the propene yield is approximately 6 times greater when they are deposited on annealed tungsten oxide as compared to HOPG substrates. Again, this observation underscores the importance of the support to prevent the cluster agglomeration. It should also be noted here that even for tungsten oxide clusters supported on annealed oxide films under this study, after annealing to 400 °C, none of the clusters studied are active toward the 2-propanol dehydration.

Size-Dependent Catalytic Activity. We now discuss the size dependence of $(WO_3)_n$ catalytic activity on the dehydration of 2-propanol. Calculated structures from several groups[31,44−46] found $(WO_3)_n$ clusters, including the $(WO_3)_1$ monomer, to contain dioxo active sites, making all of them capable, in principle, of being catalytically active.

When $(WO_3)_1$ monomers were deposited on HOPG, they heavily coalesced and displayed low catalytic activity (see Figures 6c and a(I)). In contrast, when $(WO_3)_1$ monomers were deposited on annealed tungsten oxide films they exhibited a measurable catalytic activity, suggesting a lack of aggregation (see Figure 6a(II)). Thus, we chose to compare the catalytic activity of $(WO_3)_n$ clusters deposited on annealed tungsten oxide films. Indeed, Figure 6a(II−VI) indicate that all of the $(WO_3)_n$ clusters deposited on annealed WO_3 films are catalytically active toward the dehydration of 2-propanol. Moreover, by fitting the Log[propene production per cluster] versus Log[cluster size n], a linear correlation ($N \approx 1$) was found between the cluster activity and the cluster size.

Two different mechanisms, that is, linear-scaling of active sites and cluster ripening, could explain this linear correlation.

a. Linear Scaling of Active Sites. Calculations[44] suggest that $(WO_3)_n$ clusters in the gas phase adopt a variety of structures, for example, chains, rings, or cage structures. Despite these possible isomeric structures, the most stable $(WO_3)_n$ isomers over the range of clusters studied in this previous investigation (n = 1−5) exhibit a 1:1 ratio in the number of O═W═O dioxo groups to the number of W atoms, for example, $(WO_3)_3$ contains three dioxo active sites and three W atoms. As a result, the number of active sites in a given gas phase cluster is expected to scale linearly with cluster's size, that is, with n. Although our clusters are supported on a surface and cover a wider range of cluster sizes, this linear dependency could still be operative. Additional support for the idea that the reactivity of the $(WO_3)_n$ clusters adsorbed on annealed tungsten oxide films is a reflection of a cluster size dependent reactivity can found in the systematic decrease in the propene desorption peak temperature (T_{II} = 208 °C for $(WO_3)_1$ and T_{VI} = 163 °C for $(WO_3)_{30}$ in Figure 6a) observed as the deposited cluster sizes increase.

b. Cluster Ripening. Another possibility that would explain the data shown in Figure 6a,b is that the deposited clusters aggregate and coalesce into similar-sized clusters, regardless of the initial size upon landing. In this scenario, although the size of the gas phase clusters is different, once they land onto the annealed metal oxide surface, surface ripening processes, that is, Ostwald ripening and Smoluchowski ripening, modify the size of the clusters.[47] As an example of this phenomenon, the deposition of different sized silver clusters onto HOPG results in aggregates with similar sizes due to cluster coalescence.[41] However, the observation that the peak for propene desorption temperature varies systematically with increasing initial cluster size is seemingly inconsistent with the idea that cluster ripening leads to aggregates with similar sizes. Therefore, we believe that the data shown in Figure 6b is a consequence of differences in the reactivity of individual $(WO_3)_n$ clusters.

$(MoO_3)_n$ versus $(WO_3)_n$. We also compared the dehydration of mass-selected, deposited $(MoO_3)_n$ clusters to $(WO_3)_n$ clusters. In common with studies on tungsten oxide clusters, $(MoO_3)_1$ and $(MoO_3)_3$ clusters were deposited onto HOPG but were found to be catalytically inactive (see Figure 7a,b). Size-selected $(MoO_3)_n$ clusters were also deposited onto annealed molybdenum oxide films, analogous to the studies conducted with WO_3 clusters. Figure 7a−g show that none of the $(MoO_3)_n$ clusters sizes are active toward 2-propanol dehydration regardless of the size of the cluster or nature of the support. In related studies, when Dohnálek et al. investigated the catalytic activity of $(MoO_3)_3$ clusters adsorbed on a graphene monolayer, itself grown on Pt(111), toward ethanol dehydration they also exhibited much lower catalytic activity than their $(WO_3)_3$ counterparts.[25] They ascribed this difference in the catalytic properties of WO_3 and MoO_3 clusters to the lower Lewis acidity of the metal center of $(MoO_3)_3$. Indeed, bulk studies on methanol dissociative adsorption have shown that MoO_3 is a weaker solid acid than WO_3.[48] Although theoretical calculations have found that the Lewis acidity of gas phase $(MoO_3)_n$ clusters is size dependent,[44] we discerned no obvious differences among the different $(MoO_3)_n$ cluster sizes. This suggests that any size-dependent changes in Lewis acidity of $(MoO_3)_n$ clusters are insufficient to cause these clusters to become catalytically active toward 2-propanol dehydration.

V. CONCLUSIONS

The size-dependent catalytic activity of 2-propanol dehydration on $(WO_3)_n$ and $(MoO_3)_n$ (n = 1, 2, 3, 5, 30) clusters supported on HOPG and annealed metal oxide films was studied. The ability of the support to immobilize the as-deposited clusters is suggested to play an important role in determining their catalytic activity. For $(WO_3)_n$ clusters deposited on annealed oxide films, we assert that the catalytic activity is a size-dependent effect, although it is also possible that this is a consequence of cluster ripening. For $(MoO_3)_n$ clusters, low or no dehydration activity was observed for all of the clusters investigated, an effect ascribed to the lower Lewis acidity of the $(MoO_3)_n$ as compared to the $(WO_3)_n$ clusters.

■ ASSOCIATED CONTENT

Supporting Information

Schematic of apparatus used in this study, TPR spectral deconvolution, and also an AFM image of the tungsten oxide support. This material is available free of charge via the Internet at http://pubs.acs.org.

■ AUTHOR INFORMATION

Corresponding Authors

*E-mail: howardf@jhu.edu.
*E-mail: kbowen@jhu.edu.

Notes

The authors declare no competing financial interest.

■ ACKNOWLEDGMENTS

This material is based on work supported by the Air Force Office of Scientific Research (AFOSR) under Grant No. FA9550-11-1-0068, the National Science Foundation (NSF)

under Grant No. CHE-1360692, and the Defense Threat Reduction Agency (DTRA) under Grant No. HDTRA-1-12-1-007.

REFERENCES

(1) Billas, I. M. L.; Becker, J. A.; Chatelain, A.; Deheer, W. A. Magnetic-Moments of Iron Clusters with 25 to 700 Atoms and Their Dependence on Temperature. *Phys. Rev. Lett.* **1993**, *71*, 4067−4070.

(2) Castleman, A. W.; Bowen, K. H. Clusters: Structure, Energetics, and Dynamics of Intermediate States of Matter. *J. Phys. Chem.* **1996**, *100*, 12911−12944.

(3) Landman, U.; Yoon, B.; Zhang, C.; Heiz, U.; Arenz, M. Factors in Gold Nanocatalysis: Oxidation of CO in the Non-Scalable Size Regime. *Top. Catal.* **2007**, *44*, 145−158.

(4) Yoon, B.; Hakkinen, H.; Landman, U.; Worz, A. S.; Antonietti, J. M.; Abbet, S.; Judai, K.; Heiz, U. Charging Effects on Bonding and Catalyzed Oxidation of CO on Au_8 Clusters on MgO. *Science* **2005**, *307*, 403−407.

(5) Kaden, W. E.; Wu, T. P.; Kunkel, W. A.; Anderson, S. L. Electronic Structure Controls Reactivity of Size-Selected Pd Clusters Adsorbed on TiO_2 Surfaces. *Science* **2009**, *326*, 826−829.

(6) Heiz, U.; Vanolli, F.; Trento, L.; Schneider, W. D. Chemical Reactivity of Size-Selected Supported Clusters: An Experimental Setup. *Rev. Sci. Instrum.* **1997**, *68*, 1986−1994.

(7) Jodicke, H.; Schaub, R.; Bhowmick, A.; Monot, R.; Buttet, J.; Harbich, W. Deposition of Mass-Selected Clusters Studied by Thermal Energy Atom Scattering and Low-Temperature Scanning Tunneling Microscopy: An Experimental Setup. *Rev. Sci. Instrum.* **2000**, *71*, 2818−2828.

(8) Lei, Y.; et al. Increased Silver Activity for Direct Propylene Epoxidation via Subnanometer Size Effects. *Science* **2010**, *328*, 224−228.

(9) von Issendorff, B.; Palmer, R. E. A New High Transmission Infinite Range Mass Selector for Cluster and Nanoparticle Beams. *Rev. Sci. Instrum.* **1999**, *70*, 4497−4501.

(10) Wortmann, B.; Mende, K.; Duffe, S.; Grönhagen, N.; von Issendorff, B.; Hövel, H. Ultraviolet Photoelectron Spectroscopy of Supported Mass Selected Silver Clusters. *Phys. Status Solidi B* **2010**, *247*, 1116−1121.

(11) Tong, X.; Benz, L.; Kemper, P.; Metiu, H.; Bowers, M. T.; Buratto, S. K. Intact Size-Selected Au_n Clusters on a TiO_2(110)-(1 × 1) Surface at Room Temperature. *J. Am. Chem. Soc.* **2005**, *127*, 13516−13518.

(12) Wepasnick, K. A.; Li, X.; Mangler, T.; Noessner, S.; Wolke, C.; Grossmann, M.; Gantefoer, G.; Fairbrother, D. H.; Bowen, K. H. Surface Morphologies of Size-Selected $Mo_{100\pm2.5}$ and $(MoO_3)_{67\pm1.5}$ Clusters Soft-Landed Onto HOPG. *J. Phys. Chem. C* **2011**, *115*, 12299−12307.

(13) Lin, J.; Zhou, Z.; Li, Z.; Zhang, C.; Wang, X.; Wang, K.; Gao, G.; Huang, P.; Cui, D. Biomimetic One-Pot Synthesis of Gold Nanoclusters/Nanoparticles for Targeted Tumor Cellular Dual-Modality Imaging. *Nanoscale Res. Lett.* **2013**, *8*, 170.

(14) Tamil Selvan, S.; Nogami, M.; Nakamura, A.; Hamanaka, Y. A Facile Sol−Gel Method for the Encapsulation of Gold Nanoclusters in Silica Gels and Their Optical Properties. *J. Non-Cryst. Solids* **1999**, *255*, 254−258.

(15) Liang, Z.; Khosravian, H.; Uhl, A.; Meyer, R. J.; Trenary, M. Graphene Domain Boundaries on Pt(111) as Nucleation Sites for Pt Nanocluster Formation. *Surf. Sci.* **2012**, *606*, 1643−1648.

(16) Óvári, L.; Bugyi, L.; Majzik, Z.; Berkó, A.; Kiss, J. Surface Structure and Composition of Au−Rh Bimetallic Nanoclusters on TiO_2(110): A LEIS and STM Study. *J. Phys. Chem. C* **2008**, *112*, 18011−18016.

(17) Khosravian, H.; Liang, Z.; Uhl, A.; Trenary, M.; Meyer, R. Controlled Synthesis of Rh Nanoparticles on TiO_2(110) via $Rh(CO)_2$(acac). *J. Phys. Chem. C* **2012**, *116*, 11987−11993.

(18) Moseler, M.; Walter, M.; Yoon, B.; Landman, U.; Habibpour, V.; Harding, C.; Kunz, S.; Heiz, U. Oxidation State and Symmetry of Magnesia-Supported $Pd_{13}O_x$ Nanocatalysts Influence Activation Barriers of CO Oxidation. *J. Am. Chem. Soc.* **2012**, *134*, 7690−7699.

(19) Price, S. P.; Tong, X.; Ridge, C.; Shapovalov, V.; Hu, Z. P.; Kemper, P.; Metiu, H.; Bowers, M. T.; Buratto, S. K. STM Characterization of Size-selected V_1, V_2, VO, and VO_2 Clusters on a TiO_2 (110)-(1 × 1) Surface at Room Temperature. *Surf. Sci.* **2011**, *605*, 972−976.

(20) Ferguson, G. A.; et al. Stable Subnanometer Cobalt Oxide Clusters on Ultrananocrystalline Diamond and Alumina Supports: Oxidation State and the Origin of Sintering Resistance. *J. Phys. Chem. C* **2012**, *116*, 24027−24034.

(21) Li, X.; Wepasnick, K. A.; Tang, X.; Wang, Y.; Bowen, K. H.; Fairbrother, D. H.; Gantefoer, G. Ion Induced Modification of Size-Selected MoO_3 and WO_3 Clusters Deposited on HOPG. *J. Vac. Sci. Technol. B* **2012**, *30*, 031806.

(22) Tang, X.; et al. Size Selected Clusters on Surfaces. *J. Phys. Conf. Ser.* **2013**, *438*, 012005.

(23) Kim, Y. K.; Rousseau, R.; Kay, B. D.; White, J. M.; Dohnalek, Z. Catalytic Dehydration of 2-Propanol on $(WO_3)_3$ Clusters on TiO_2(110). *J. Am. Chem. Soc.* **2008**, *130*, 5059−5061.

(24) Li, S. C.; Li, Z. J.; Zhang, Z. R.; Kay, B. D.; Rousseau, R.; Dohnalek, Z. Preparation, Characterization, and Catalytic Properties of Tungsten Trioxide Cyclic Trimers on FeO(111)/Pt(111). *J. Phys. Chem. C* **2012**, *116*, 908−916.

(25) Li, Z. J.; Fang, Z. T.; Kelley, M. S.; Kay, B. D.; Rousseau, R.; Dohnalek, Z.; Dixon, D. A. Ethanol Conversion on Cyclic $(MO_3)_3$ (M = Mo, W) Clusters. *J. Phys. Chem. C* **2014**, *118*, 4869−4877.

(26) Li, Z. J.; Smid, B.; Kim, Y. K.; Matolin, V.; Kay, B. D.; Rousseau, R.; Dohnalek, Z. Alcohol Dehydration on Monooxo W=O and Dioxo O=W=O Species. *J. Phys. Chem. Lett.* **2012**, *3*, 2168−2172.

(27) Rousseau, R.; Dixon, D. A.; Kay, B. D.; Dohnalek, Z. Dehydration, Dehydrogenation, and Condensation of Alcohols on Supported Oxide Catalysts Based on Cyclic $(WO_3)_3$ and $(MoO_3)_3$ Clusters. *Chem. Soc. Rev.* **2014**, in press.

(28) Rothgeb, D. W.; Mann, J. E.; Jarrold, C. C. H_2 Production from Reactions Between Water and Small Molybdenum Suboxide Cluster Anions. *J. Chem. Phys.* **2010**, *133*, 054305.

(29) Huang, X.; Zhai, H. J.; Kiran, B.; Wang, L. S. Observation of d-Orbital Aromaticity. *Angew. Chem., Int. Ed.* **2005**, *44*, 7251−7254.

(30) Huang, X.; Zhai, H. J.; Waters, T.; Li, J.; Wang, L. S. Experimental and Theoretical Characterization of Superoxide Complexes $[W_2O_6(O_2^-)]$ and $[W_3O_9(O_2^-)]$: Models for the Interaction of O_2 with Reduced W Sites on Tungsten Oxide Surfaces. *Angew. Chem., Int. Ed.* **2006**, *45*, 657−660.

(31) Sun, Q.; Rao, B. K.; Jena, P.; Stolcic, D.; Kim, Y. D.; Gantefor, G.; Castleman, A. W. Appearance of Bulk Properties in Small Tungsten Oxide Clusters. *J. Chem. Phys.* **2005**, *122*, 9417−9422.

(32) Zhai, H. J.; Kiran, B.; Cui, L. F.; Li, X.; Dixon, D. A.; Wang, L. S. Electronic Structure and Chemical Bonding in MO_n^- and MO_n Clusters (M = Mo, W; n = 3−5): A Photoelectron Spectroscopy and ab initio Study. *J. Am. Chem. Soc.* **2004**, *126*, 16134−16141.

(33) Hammer, B.; Nørskov, J. K. Theoretical Surface Science and Catalysis: Calculations and Concepts. In *Adv. Catal.*; Bruce, C., Gates, H. K., Eds.; Academic Press: New York, 2000; Vol. *45*, pp 71−129.

(34) Somorjai, G. A.; Carrazza, J. Structure Sensitivity of Catalytic Reactions. *Ind. Eng. Chem. Fundam.* **1986**, *25*, 63−69.

(35) Bonanni, S.; Aït-Mansour, K.; Harbich, W.; Brune, H. Effect of the TiO_2 Reduction State on the Catalytic CO Oxidation on Deposited Size-Selected Pt Clusters. *J. Am. Chem. Soc.* **2012**, *134*, 3445−3450.

(36) Jensen, P. Growth of Nanostructures by Cluster Deposition: Experiments and Simple Models. *Rev. Mod. Phys.* **1999**, *71*, 1695−1735.

(37) Xie, F. Y.; Gong, L.; Liu, X.; Chen, J.; Xie, W. G.; Zhang, W. H.; Chen, S. H. Preparation and Characterization of the Amorphous Tungsten Cone Field Emitter Arrays by Ar^+ Etching. *Appl. Surf. Sci.* **2009**, *256*, 693−697.

(38) Werfel, F.; Minni, E. Photoemission Study of the Electronic Structure of Mo and Mo Oxides. *J. Phys. C: Solid State Phys.* **1983**, *16*, 6091−6100.
(39) Falconer, J. L.; Schwarz, J. A. Temperature-Programmed Desorption and Reaction: Applications to Supported Catalysts. *Catal. Rev. Sci. Eng.* **1983**, *25*, 141−227.
(40) The exact value cannot be more accurately determined because any propene signal from $(WO_3)_1$/HOPG is on the same scale as the background noise.
(41) Goldby, I. M.; Kuipers, L.; von Issendorff, B.; Palmer, R. E. Diffusion and Aggregation of Size-Selected Silver Clusters on a Graphite Surface. *Appl. Phys. Lett.* **1996**, *69*, 2819−2821.
(42) Carroll, S. J.; Weibel, P.; Issendorff, B. v.; Kuipers, L.; Palmer, R. E. The Impact of Size-Selected Ag Clusters on Graphite: An STM Study. *J. Phys.: Condens. Matter* **1996**, *8*, L617−L624.
(43) Bondarchuk, O.; Huang, X.; Kim, J.; Kay, B. D.; Wang, L. S.; White, J. M.; Dohnalek, Z. Formation of Monodisperse $(WO_3)_3$ Clusters on TiO_2(110). *Angew. Chem., Int. Ed.* **2006**, *45*, 4786−4789.
(44) Li, S. G.; Dixon, D. A. Molecular and Electronic Structures, Brönsted Basicities, and Lewis Acidities of Group VIB Transition Metal Oxide Clusters. *J. Phys. Chem. A* **2006**, *110*, 6231−6244.
(45) Sai, L.; Tang, L.; Huang, X.; Chen, G.; Zhao, J.; Wang, J. Lowest-Energy Structures of $(WO_3)_n$ $(2 \leq n \leq 12)$ Clusters from First-Principles Global Search. *Chem. Phys. Lett.* **2012**, *544*, 7−12.
(46) Wang, B.; Chen, W. J.; Zhao, B. C.; Zhang, Y. F.; Huang, X. Tetratungsten Oxide Clusters $W_4O_n^{-/0}$ (n = 10−13): Structural Evolution and Chemical Bonding. *J. Phys. Chem. A* **2010**, *114*, 1964−1972.
(47) Fukamori, Y.; Konig, M.; Yoon, B.; Wang, B.; Esch, F.; Heiz, U.; Landman, U. Fundamental Insight Into the Substrate-Dependent Ripening of Monodisperse Clusters. *ChemCatChem* **2013**, *5*, 3330−3341.
(48) Badlani, M.; Wachs, I. Methanol: A "Smart" Chemical Probe Molecule. *Catal. Lett.* **2001**, *75*, 137−149.